Xi'an Shiyou Daxue Xuebao (Ziran Kexue Ban)/
Journal of Xi'an Shiyou University, Natural Sciences Edition
ISSN: 1673-064X
E-Publication: Online Open Access
Vol: 67 Issue 03 | 2024
DOI: 10.5281/zenodo.10867807

OPTICAL LOOP ARCHITECTURE FOR ULTRA-FAST OPTICAL SWITCHING SERVICE AND EFFICIENT BUFFER

VIVEKANAND MISHRA*
Assistant Professor, Department of Science, Alliance University, Bengaluru.
*Corresponding Author Email: vivekanand.mishra@alliance.edu.in

RASHMI
Assistant Professor, Department of Science, Alliance University, Bengaluru.
Email: rashmi.sinha@alliance.edu.in

CHANDNI PATHAK
Assistant Professor, Department of Science, Alliance University, Bengaluru.
Email: chandni.pathak@alliance.edu.in

SUKRITI
Assistant Professor, Department of Physics, GLA University, Mathura, Uttar Pradesh.
Email: sukriti.gla@gla.ac.in

Abstract

The integration of optical data storage using fiber loops and ultra-fast optical switching via nonlinear optical loop mirrors (NOLMs) has long been recognized as an optimal approach for all-optical processing. This article presents a novel integration of these technologies to create an efficient buffering-switching device aimed at mitigating signal contention. Through thorough analysis, we explore the limitations of this integrated device in achieving error-free processing across multiple buffering cycles. Various factors, such as different types of noise leading to intensity fluctuations in buffered and demultiplexed signals, are assessed. Additionally, we delve into the switching characteristics of the NOLM demultiplexer to provide a comprehensive understanding of the device's performance.

1. INTRODUCTION

The increasing demand for high transmission rates in telecommunications networks has sparked significant interest in optical communications. Direct transmission of optical signals within the optical layer, without the need for electro-optical-electrical (OEO) conversion, has surfaced as a implying technology for advancing optical networks. Accordingly, all-optical processing plays a pivotal role in shaping the outlook of optical communication networks. However, signal contention poses a major challenge due to the absence of optical RAM. Various techniques, including the use of fiber delay lines (FDLs) for storage, have been proposed to address this issue. Yet, longer FDLs are required for significant buffering times, leading to the development of techniques based on fiber loop recirculation [1, 3, 4, 5]. By allowing optical signals to recirculate within a fiber loop until needed for transmission, these techniques offer a more compact buffer solution compared to FDLs. The nonlinear optical loop mirror (NOLM) has demonstrated efficiency as an optical demultiplexer, enabling high-speed switching. This article [6,7] proposes the integration of an optical loop buffer (OLB) with NOLM to create an efficient buffering-

Xi'an Shiyou Daxue Xuebao (Ziran Kexue Ban)/
Journal of Xi'an Shiyou University, Natural Sciences Edition
ISSN: 1673-064X
E-Publication: Online Open Access
Vol: 67 Issue 03 | 2024
DOI: 10.5281/zenodo.10867807

switching device for managing signal contention. The analysis considers various types of noise within the proposed device to optimize loop circulations for buffering. Additionally, adverse impacts within the NOLM switch, such as group velocity dispersion (GVD) and pulse walk-off, which affect signal transmission and reflection, are investigated.

2. SYSTEM MODEL

The concept of the nonlinear optical loop mirror (NOLM) demultiplexer has grown from the Sagnac interferometer, offering superior switching speeds, albeit with subdued operating power requirements and minimal framework compared to alternatives. In a NOLM demultiplexer, the elevated-intensity control signal from the Wavelength Division Multiplexing (WDM) coupler induces a Cross-Phase Modulation (XPM) upshot on the clockwise input signal [8-11], leading to a refractive index variation due to the Kerr effect and subsequent signal phase shift. Constructing the NOLM demultiplexer requires a longer fiber loop due to the small nonlinear parameter (γ) of the fiber, necessitating a loop length of 3 km to induce a phase shift of π.

Traditional optical communication lacks an all-optical buffer device and implementing Fiber Delay Lines (FDLs) for extended buffering periods is impractical. Consequently, the optical loop buffer (OLB), which shares a similar architecture with the NOLM switch, is ideal for buffering services. Unlike the NOLM switch, the OLB does not require signal splitting for co-propagation, thereby avoiding issues like unsought XPM and pulse walk-off. The OLB allows for multiple signal recirculations until needed for transmission, with a maximum buffer time per loop calculated as $T_{max} = \frac{nl}{c}$, [11-16] providing three microseconds of buffer time in this experiment. However, excessive recirculation may have adverse effects.

Combining the NOLM demultiplexer with the OLB offers robust optical buffering-switching assistance for optical networks [17-18]. Placing the OLB beforehand the NOLM switch reduces contention and minimizes the quantity of reflected signals. When an input signal appears at the switch, it is routed based on its buffering needs. Signals requiring immediate transmission bypass the OLB and enter the NOLM switch directly, while those needing buffering are directed into the OLB. The OLB utilizes a 100:0 coupler to ensure unidirectional signal recirculation within the loop, with an optical amplifier compensating for loop losses and an optical isolator enforcing one-way traffic.

Buffered signals are recirculated within the OLB until required by NOLM for transmission. Unlike the NOLM switch in previous research, the NOLM demultiplexer in this setup utilizes a Semiconductor Optical Amplifier (SOA) to induce optical nonlinearity, eliminating dependence on SOA gain saturation. The high-intensity control signal couples with the clockwise signal, inducing a phase shift and facilitating signal switching toward the optical receiver when a phase difference of π is achieved connecting the counter-propagating signals [19-20].

Xi'an Shiyou Daxue Xuebao (Ziran Kexue Ban)/
Journal of Xi'an Shiyou University, Natural Sciences Edition
ISSN: 1673-064X
E-Publication: Online Open Access
Vol: 67 Issue 03 | 2024
DOI: 10.5281/zenodo.10867807

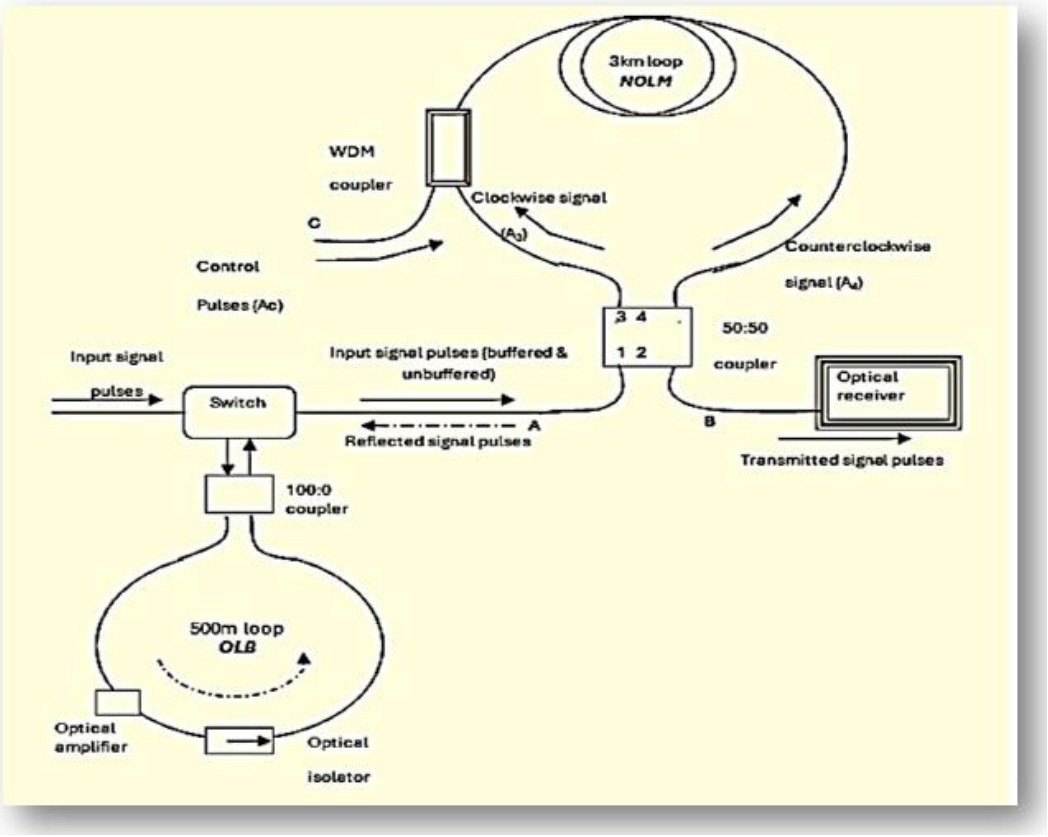

Fig 1: Schematic diagram of an OLB combined with the NOLM switch

3. THEORETICAL INVESTIGATION

While the suggested optical buffering and switching device promises to enhance signal throughput in optical networks, the demultiplexed signal remains susceptible to degradation from various noise sources. These include thermal noise, shot noise, and different classes of beat noise associated with spontaneous emission (ASE noise may also contribute).

Within the Optical Loop Buffer (OLB), the signal recirculates within the fiber loop for a defined number of sequences, resulting in noise accumulation with each circulation. The decrease in obtained power at the receiver after recirculation, denoted as Ps, is determined by the equation:

$$P_S = P_N 10^{-z/10} \quad [1]$$

Amount where P_N and z represents the output power after N loops of circulation, and z indicates the quantity of data signal attenuation in decibels (dB). Ps serves as the input signal power for the buffered signal entering the NOLM switch.

Xi'an Shiyou Daxue Xuebao (Ziran Kexue Ban)/
Journal of Xi'an Shiyou University, Natural Sciences Edition
ISSN: 1673-064X
E-Publication: Online Open Access
Vol: 67 Issue 03 | 2024
DOI: 10.5281/zenodo.10867807

Upon entering the NOLM switch, the input signal is equally split by a 50:50 coupler and co-propagates bidirectionally. The behaviour of the input signal and control pulse is headed by the nonlinear Schrödinger (NLS) equation. This equation is particularly applicable when a extended length of fiber is used, as dispersive and nonlinear effects become substantial over longer distances. Thus, the signals propagating clockwise, counter clockwise, and the control pulse satisfying the NLS equation can be expressed as:

$$\frac{\partial A_3}{\partial z} + \frac{i\beta_{2s}}{2}\frac{\partial^2 A_3}{\partial T^2} = i\gamma_s(|A_3|^2 + 2|A_c|^2)A_3 \quad [2]$$

$$\frac{\partial A_c}{\partial z} + \beta_1\frac{\partial A_C}{\partial T} + \frac{i\beta_{2c}}{2}\frac{\partial^2 A_c}{\partial T^2} = i\gamma_c(|A_c|^2 + 2|A_3|^2)A_c \quad [3]$$

$$\frac{\partial A_4}{\partial z} + \frac{i\beta_{2s}}{2}\frac{\partial^2 A_4}{\partial T^2} = i\gamma_{sc}|A_4|^2 A_4 \quad [4]$$

Where z represents the distance from port three beside the clockwise direction, β_{2s} and β_{2c} denote the Group Velocity Dispersion (GVD) parameters for the signal and control pulses, correspondingly. T is the time variable in the retarded frame *T*, γ_s and γ_c while signify the nonlinear coefficient parameters of the signal and control pulses, respectively.

Additionally, the signal pulses in the clockwise direction (A_3), counterclockwise direction (A_4) and the control pulse (A_c) are listed as follows:

$$A_3 = (1-K)^{1/2}(P_1)^{1/2}(P_0)^{1/2}e^{-t^2/2\,(T_{01})^4} \quad [5]$$

$$A_4 = j(K)^{1/2}(P_1)^{1/2}(P_0)^{1/2}e^{-t^2/2\,(T_{01})^4} \quad [6]$$

$$A_c = (P_2)^{1/2}(P_0)^{1/2}e^{-t^2/2\,(T_{02})^4} \quad [7]$$

In this equation, *K* denotes the coupling ratio, P_1 and P_2 represent the peak power for the signal pulse and control pulse, respectively, P_0 stands for the input power, *t* denotes the time variable, is the time variable, $T_{01}$and t corresponds to the full width at half maximum (FWHM) for the signal pulse.

The control pulse originating from the Wavelength Division Multiplexing (WDM) coupler couples and co-propagates with the anticipated section of the clockwise-propagating signal intended for transmission. The signal pulse transmitted out of the fiber loop is expressed as:

$$signal\ out = (1-K)^{1/2}E_4 + j(K)^{1/2}E_1 \quad [8]$$

Where E_1 and E_4 correspond to the clockwise and counterclockwise propagating signals correspondingly. Here, denote the clockwise and counterclockwise propagating signals, respectively. These values are determined numerically by employing the split-step Fourier method (SSFM).

Xi'an Shiyou Daxue Xuebao (Ziran Kexue Ban)/
Journal of Xi'an Shiyou University, Natural Sciences Edition
ISSN: 1673-064X
E-Publication: Online Open Access
Vol: 67 Issue 03 | 2024
DOI: 10.5281/zenodo.10867807

Devoid of any control pulse coupled into the fiber loop, mutually the clockwise and counterclockwise propagating signals remain unaffected in terms of phase difference. As a result, the input signal reflects back after traversing the loop. The reflected signal pulse is formulated as:

$$signal\ reflect = j(K)^{1/2}E_4 + j(1-K)^{1/2}E_1 \qquad [9]$$

Therefore, the transmittance (*υ*) of the NOLM demultiplexer can be derived from:

$$\upsilon = \frac{|signal\_out|^2}{|signal\_input|^2} \qquad [10]$$

The analysis of Bit Error Rate (BER) is employed to assess signal deprivation associated with NOLM demultiplexing. The variance of thermal noise and shot noise can be determined from:

$$\sigma_{th}^2 = 4kTB/R_L \qquad [11]$$

$$\sigma_{sh\_a}^2 = 2qI_rB \qquad [12]$$

Where *k* and *q* have fixed values, representing Boltzmann's constant and electron charge respectively, *T* indicates the temperature, *B* is electrical bandwidth, R_L is load resistance of the photodiode, I_r is the photocurrent generated at the receiver. For signal 0 and 1, I_r becomes I_0 and I_1 respectively.

Moreover, various types of spontaneous beat noise stemming from the preamplifier have led to certain shortcomings in the output signals. These include beat noise between the signal and spontaneous emission, spontaneous emission against itself, and shot noise against spontaneous emission. The interaction between the signal and spontaneous emission arises from their disparate optical frequencies.

Where k and q are constants representing Boltzmann's constant and electron charge respectively, T denotes the temperature, B stands for electrical bandwidth, R_L represents the load resistance of the photodiode, and I_r denotes the photocurrent generated at the receiver. When considering signals 0 and 1, I_r takes on the values of I_0 and I_1 respectively.

Additionally, the output signals are affected by various types of spontaneous beat noise originating from the preamplifier. These noise types include beat noise between the signal and spontaneous emission, spontaneous emission interfering with itself, and shot noise conflicting with spontaneous emission. The interaction between the signal and spontaneous emission arises from their differing optical frequencies.

However, inter-beating among the spontaneous emissions occurs due to their wide frequency range governed by their effective bandwidth. Consequently, current fluctuations resulting from these inter-beatings produce beat noise, which in turn degrades the signal.

Xi'an Shiyou Daxue Xuebao (Ziran Kexue Ban)/
Journal of Xi'an Shiyou University, Natural Sciences Edition
ISSN: 1673-064X
E-Publication: Online Open Access
Vol: 67 Issue 03 | 2024
DOI: 10.5281/zenodo.10867807

For NOLM operations, the variances of the aforementioned beat noise are outlined below:

$$\sigma^2_{sg\_spn\_r} = 4R^2 G_p S_{sp} B\overline{N_r} \quad [13]$$

$$\sigma^2_{sg\_spn} = 4R^2 S_{sp} f B \quad [14]$$

$$\sigma^2_{sh\_spn} = 4qRS_{sp} f B \quad [15]$$

Where *f* is the receiver optical bandwidth and the spontaneous emission noise spectral density (S_{sp}) is given by:

$$S_{sp} = (G-1) n_{sp} hf \quad [16]$$

G and *h* signify the optical amplifier gain and Planck's constant respectively, and n_{sp} is the spontaneous emission factor. The mean photon number $(\overline{N_r})$ for signals 0 and 1 will become $\overline{N_0}$ and N_1 respectively. Both the value of I_r and $\overline{N_r}$ have been assessed, taking into account the impacts of Group Velocity Dispersion (GVD), pulse walk-off between the signal and control pulse, as well as channel and intrinsic crosstalk on the demultiplexed signals. Channel crosstalk occurs when an undesired channel is switched to the output port during demultiplexing, typically due to the switching window overlapping into adjacent signal pulses. Conversely, intrinsic crosstalk manifests as a small amount of leakage signal at the output, even in the absence of any control signal within the NOLM.

Thus, $\overline{N_0}$ and N_1 of the demultiplexed signals are given by:

$$\overline{N_1} = \overline{N_s}\,[1 + CX(F_{TDM} - 1)(R_1 + E_r + E_r R_1)] \quad [17]$$

$$\overline{N_0} = \overline{N_s}\,[E_r + CX(F_{TDM} - 1)(R_1 + E_r - E_r R_1)] \quad [18]$$

Where F_{TDM} is the TDM factor, $R_1$is the signal's mark ratio, E_r is the intensity modulator's extinction ratio in the optical transmitter, $\overline{N_s}$ represents the mean photon number when only the "1" bits present, CX is the channel crosstalk. CX is related to intrinsic crosstalk (*IX*) and can be written as:

$$CX = 1 - (1 - IX)\cos\left[\frac{\pi}{2(E-1)}\right]^2 \quad [19]$$

Where

$$E = \frac{1}{f_c \beta_1} erf\left(\frac{\beta_1 \sqrt{\ln 2}}{T_{02}}\right) \quad [20]$$

T_{02} represents the full width at half maximum (FWHM) for the control pulse, β_1 stands for the walk-off parameter, f_c denotes the control pulse repetition rate.

Xi'an Shiyou Daxue Xuebao (Ziran Kexue Ban)/
Journal of Xi'an Shiyou University, Natural Sciences Edition
ISSN: 1673-064X
E-Publication: Online Open Access
Vol: 67 Issue 03 | 2024
DOI: 10.5281/zenodo.10867807

Additionally, owing to intensity fluctuations induced by the timing jitter between the control and input signals, the relative intensity noise variance for signal 0 and 1 will be incorporated into the analysis of the NOLM demultiplexer and is expressed as:

$$\sigma_{RIN\_0}^2 = \left(q\eta G_p\right)^2 [RIN\left(\overline{N_0}\right)^2 B + RIN_{NOLM}\left(Er\right)^2\left(\overline{N_s}\right)^2] \quad (21)$$

$$\sigma_{RIN\_1}^2 = \left(q\eta G_p\right)^2 [RIN\left(\overline{N_1}\right)^2 B + RIN_{NOLM}\left(\overline{N_s}\right)^2] \quad (22)$$

where η represents the photodetector quantum efficiency, *RIN* and RIN_{NOLM} signify the optical signal source relative intensity noise and intensity fluctuations resulting from NOLM demultiplexing contribute to the current fluctuation variance in the NOLM switch, expressed as:

$$\sigma_q^2 = \sigma_{th}^2 + \sigma_{sh\_a}^2 + \sigma_{sg-spn\_r}^2 + \sigma_{spn-spn}^2 + \sigma_{sh-spn}^2 + \sigma_{RIN\_0}^2 + \sigma_{RIN\_1}^2 \quad (23)$$

For signal 0 and 1 in the NOLM analysis, σ_q^2 in Eq. (23) will be swapped with σ_0^2 and σ_1^2 correspondingly. To assess signals that have undergone the optical buffering and switching devices, the utilized Bit Error Rate (BER) will be provided as:

$$BER = \frac{1}{2} erfc\left[\frac{I_1}{\sqrt{2}(\sigma_1+\sigma_0)}\right] \quad [24]$$

Where I1=RP_{1a} and P_{1a} represent the output power from the switch.

4. RESULT AND DISCUSSION

We perform a numerical evaluation to ensure error-free optical buffering-switching service utilizing the system model depicted in Figure 1.

The elementary objective of the two ensuing outcomes is to ascertain the highest recirculation capacity for data packets comprising 512 bits each.

Figure 2 displays the BER investigation of the buffered signal across several loop recirculation within the OLB. Subsequently, Figure 3 depicts the BER investigation for the buffered signal post-demultiplexing by the NOLM switch. Both experiments maintain the following parameters: a data rate of 10 Gbps.

$E_r = -25, \eta = 0.7, T = 293\ K, f = 374\ GHz, B = \frac{1}{2}\ (data\ rate), R = 0.9, RIN = 10^{-15}, RIN_{NOLM} = 1^{-3}, T_0 = 5^{-12}$.

Xi'an Shiyou Daxue Xuebao (Ziran Kexue Ban)/
Journal of Xi'an Shiyou University, Natural Sciences Edition
ISSN: 1673-064X
E-Publication: Online Open Access
Vol: 67 Issue 03 | 2024
DOI: 10.5281/zenodo.10867807

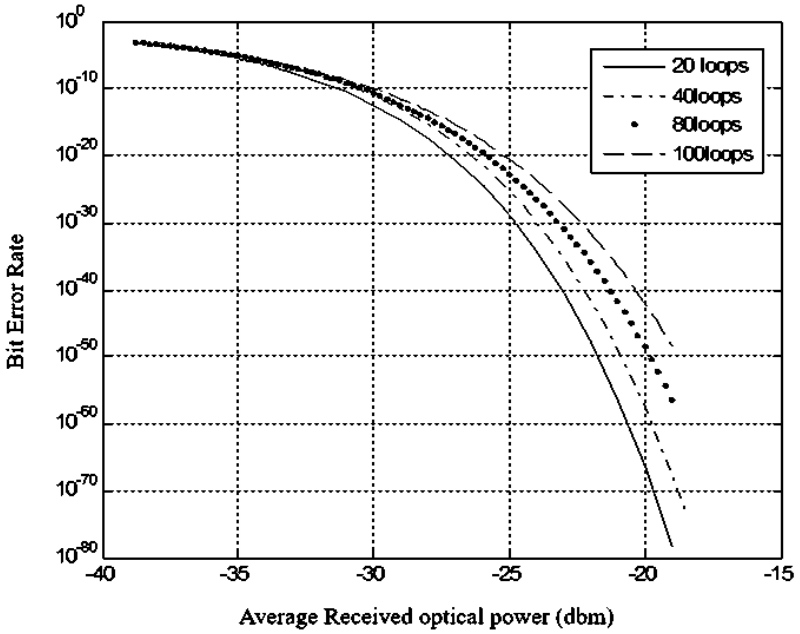

Fig 2: BER plotted against gathered optical power for different loop recirculations within the buffering device

Figure 2 illustrates that the input signal undergoing 20 circulations within the buffer outperformed other investigations with elevated loop circulations. With an increase in the number of circulations, the BER deteriorates further. This outcome is primarily attributed to signal intensity fluctuations produced by numerous noise sources, as previously discussed. Based on the maximum buffering timeT_{max}, a hundred loop circulations within the OLB provide roughly three hundred microseconds of optical buffering time, maintaining error-free processing capability.

As the signal prepares for transmission, it progresses towards the NOLM demultiplexer, where the buffered signal experiences swift nonlinear switching. Figure 3 presents a BER analysis for different quantities of loop-buffered signals undergoing NOLM demultiplexing at a 10 Gbps data rate, while Figure 4 expands this analysis to a 20 Gbps data rate. Notably, as the data rate increases, there's a deterioration in BER performance. Simulated results indicate a marked decline in BER performance for demultiplexed signals compared to the analysis in Figure 2. This decline can be attributed to various noise sources encountered within the OLB, alongside several nonlinear effects, including GVD, pulse walk-off, channel, and intrinsic crosstalk. Nevertheless, despite these challenges, the findings suggest that signals passing through the proposed model can withstand up to one hundred loop circulations while staying within a reasonably received optical power range.

Xi'an Shiyou Daxue Xuebao (Ziran Kexue Ban)/
Journal of Xi'an Shiyou University, Natural Sciences Edition
ISSN: 1673-064X
E-Publication: Online Open Access
Vol: 67 Issue 03 | 2024
DOI: 10.5281/zenodo.10867807

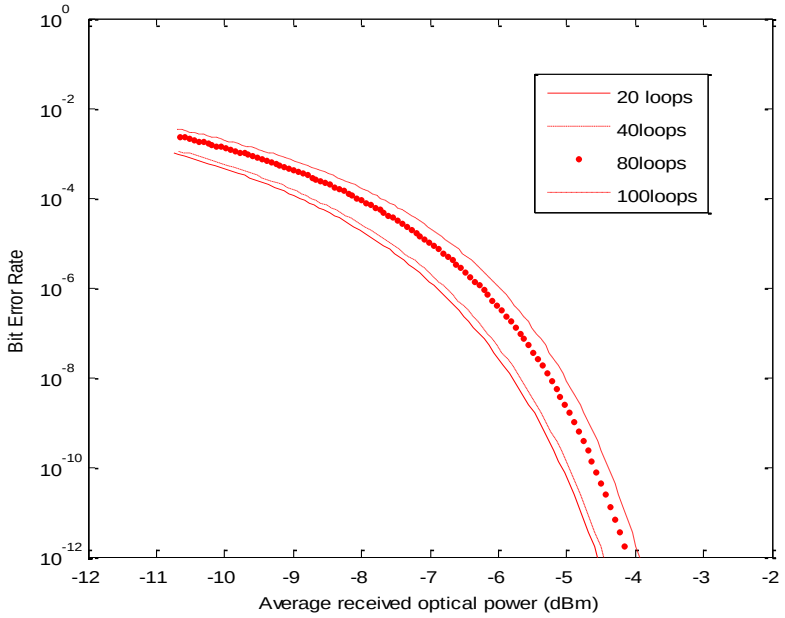

Fig 3: Bit Error Rate (BER) compared to received optical power across different loop recirculations for both the buffering device and NOLM demultiplexing at a data rate of 10 Gbps

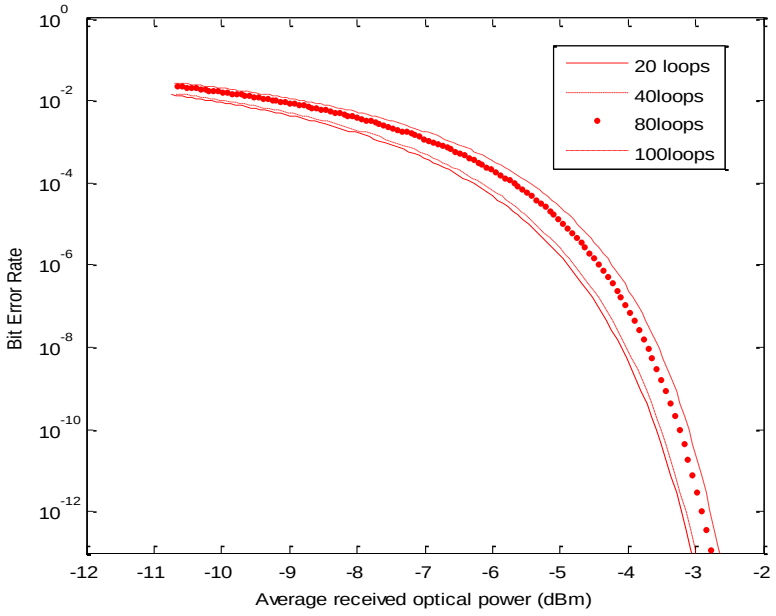

Fig 4: Bit Error Rate (BER) versus optical power with varying loop recirculation for both the buffering device and demultiplexing by NOLM at a data rate of 20 Gbps

Xi'an Shiyou Daxue Xuebao (Ziran Kexue Ban)/
Journal of Xi'an Shiyou University, Natural Sciences Edition
ISSN: 1673-064X
E-Publication: Online Open Access
Vol: 67 Issue 03 | 2024
DOI: 10.5281/zenodo.10867807

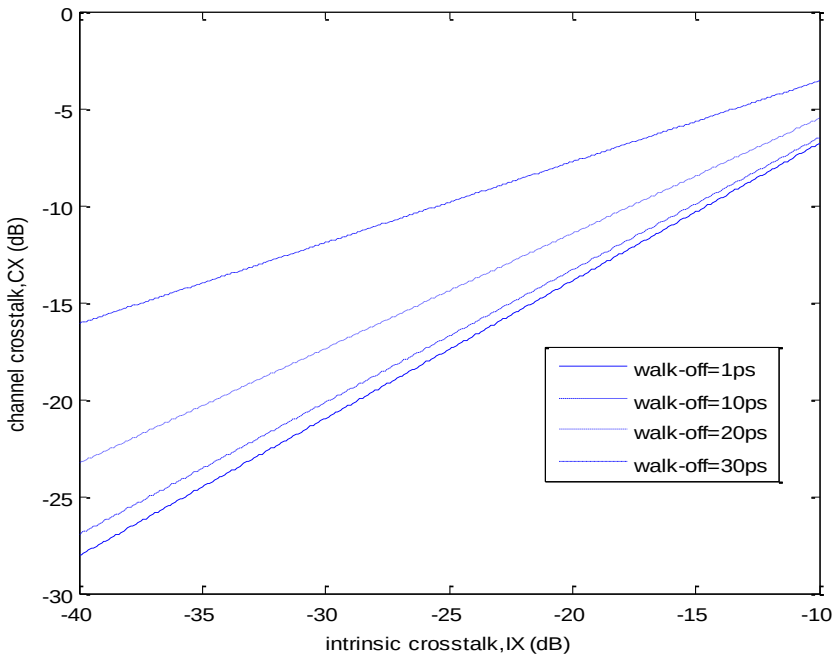

Fig 5: Comparison of channel crosstalk versus intrinsic crosstalk across different levels of pulse walk-off

Figure 5 presents simulated results demonstrating the relationship between the channel and intrinsic crosstalk at different levels of pulse walk-off between the control and signals. It is evident that higher levels of walk-off lead to an increase in the minimum value of channel crosstalk relative to intrinsic crosstalk.

This observation confirms that pulse walk-off contributes to heightened channel crosstalk, thereby impacting the quality of demultiplexed signals. Several unchanged parameters utilized in Fig. 6 and Fig. 7 are as follows: K=0.5, $T_{01} = 3ps, T_{02} = 4ps.$

Figure 6 depicts the signal waveform propagating in the NOLM switch under conditions where Group Velocity Dispersion (GVD) and pulse walk-off are negligible. The signals are tightly concentrated within the switching profile.

However, in practical scenarios, NOLM switches experience higher values of GVD and pulse walk-off, leading to signal broadening and deviation from the central position, as illustrated in Figure 7. This phenomenon compromises switching efficiency, consequently affecting the Bit Error Rate (BER) performance, as demonstrated in Figure 3.

Xi'an Shiyou Daxue Xuebao (Ziran Kexue Ban)/
Journal of Xi'an Shiyou University, Natural Sciences Edition
ISSN: 1673-064X
E-Publication: Online Open Access
Vol: 67 Issue 03 | 2024
DOI: 10.5281/zenodo.10867807

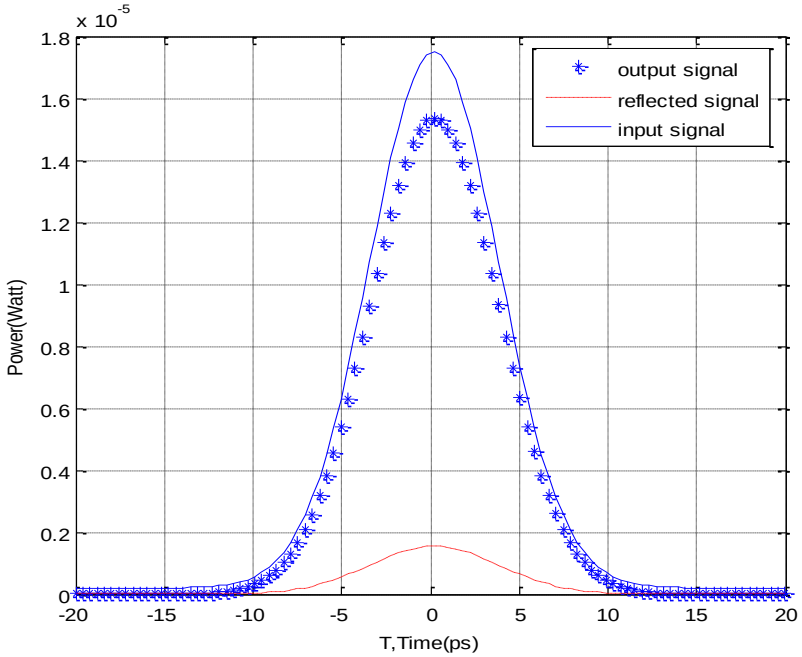

Fig 6: Signal waveform for NOLM with minimal Group Velocity Dispersion (GVD) and pulse walk-off

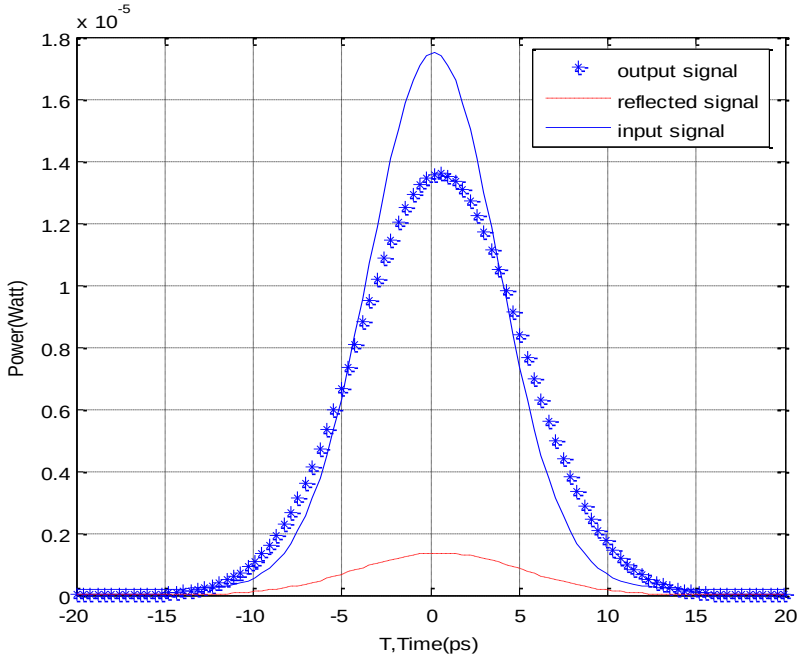

Fig 7: Signal waveform for NOLM with increased Group Velocity Dispersion (GVD) and pulse walk-off

Xi'an Shiyou Daxue Xuebao (Ziran Kexue Ban)/
Journal of Xi'an Shiyou University, Natural Sciences Edition
ISSN: 1673-064X
E-Publication: Online Open Access
Vol: 67 Issue 03 | 2024
DOI: 10.5281/zenodo.10867807

5. CONCLUSIONS

This paper presents a new optical buffering-switching device, utilizing an optical fiber loop architecture to provide a compact and efficient optical buffer with rapid switching capabilities. Simulation results indicate that signals traveling through the fiber loops experience intensity fluctuations due to various noise sources. Furthermore, phenomena like Group Velocity Dispersion (GVD), pulse walk-off, channel crosstalk, and intrinsic crosstalk during NOLM demultiplexing contribute to the degradation of signal quality. GVD and pulse walk-off cause pulse broadening and signal deviation within the NOLM, exacerbating channel crosstalk and signal degradation. As noise accumulates with each loop circulation, the Bit Error Rate (BER) increases with the number of recirculations. However, simulations suggest that signals can circulate within the buffer loop for up to one hundred rounds before being demultiplexed by the NOLM switch.

Reference

1) A. Bogris, "An All-Optical Buffer Based on Non-Degenerate Phase-Sensitive Parametric Amplification", Journal of Lightwave Technology, vol.36, pp.5949-5955, 2018.

2) M. F. Tang, F. M. Abbou, A. Abid, V. N. Mishra, and H. T. Chuah, "Packet loss rate of an optical burst switch with nonlinear optical loop mirrors," IEICE Electronics Express, vol. 3, no.11, pp. 243-248, 2006.

3) G. P. Agrawal, Fiber-Optic Communication Systems, Wiley-Interscience Publication, N.Y., 1997.

4) D. Grendar, O. Pottiez, M. Dado, J. Müllerova, J. Dubovan "Effect of control-beam polarization and power on optical time-domain demultiplexing in a new nonlinear optical loop mirror design," Optical Engineering, Vol. 48, pp. 055002, 2009.

5) A. Bogoni, "Nonlinear optical loop mirrors: investigation solution and experimental validation for undesirable counterpropagating effects in all-optical signal processing," IEEE J. Sel. Topics in Quantum Electron. 10, 5 (2004): 1115-1123.

6) T. Sakamoto et al, "All-optical wavelength conversion of 500-fs pulse trains by using a nonlinear-optical loop mirror composed of a highly nonlinear DSF," IEEE Photon. Technol. Lett. 13, 5 (2001): 502-504.

7) T. Huanget al, "Photonic generation of UWB pulses using a nonlinear optical loop mirror and its distribution over a fiber link," IEEE Photon.Technol. Lett. 23, 17 (2011): 1255-1257.

8) B. G. Lee et al, "All-optical regeneration and demultiplexing for 160 Gb/s transmission systems using a NOLM-based three-stage scheme," IEEE J. Sel. Topics in Quantum Electron. 10, 1 (2004): 192-196.

9) J. Leuthold et al., "Nonlinear silicon photonics," Nat. Photonics 4" (2010): 535.

10) A. Bononi et al., "Nonlinear optical loop mirrors: inverstigation solution an experimental validation for undesirable counterpropagating effects in all-optical signal processing," IEEE J. Sel. Topics in Quantum Electron. 10, 5 (2004): 1115-1123.

11) Morsy, M.H.S.; Sowailem, M.Y.S.; Shalaby, H.M.H. Upper and lower bounds of burst loss probability for a core node in an Optical Burst Switched network with Pareto distributed arrivals. In Proceedings of the IEEE 17th International Conference on Telecommunications, Doha, Qatar, 4–7 April 2010; pp. 523–527.

12) Lou, H.L. Implementing the Viterbi Algorithm. IEEE Signal Proc. Magaz. 1995, 5, 42–52. [Google Scholar]

ISSN: 1673-064X
E-Publication: Online Open Access
Vol: 67 Issue 03 | 2024
DOI: 10.5281/zenodo.10867807

13) R Core Team: R: A Language and Environment for Statistical Computing. R Foundation for Statistical Computing. 2021. Available online: https://www.R-project.org/ (accessed on 10 December 2021).

14) Rivera-Lara, E.J.; Herreriás-Hernández, R.; Pérez-Diáz, J.A.; Garcá-Hernández, C.F. Analysis of the Relationship between QoS and SNR for an 802.11g WLAN. In Proceedings of the International Confererence on Communication Theory, Reliability, and Quality of Service, Bucharest, Romania, 29 June–5 July 2008; pp. 103–107. [Google Scholar]

15) Liu, R.P.; Sutton, G.J.; Yang, X.; Collings, I.B. Modelling QoS Performance of IEEE 802.11 DCF under Practical Channel Fading Conditions. IEEE Intern. Confer. Commun. 2011, 1, 1–6.

16) Karmakar, R.; Chattopadhyay, S.; Chakraborty, S. Dynamic Link Adaptation in IEEE 802.11ac: A Distributed Learning Based Approach. In Proceedings of the IEEE 41st Conference on Local Computer Networks Workshops, Dubai, United Arab Emirates, 7–10 November 2016; pp. 87–94.

17) Mukherjee, S.; Peng, X.; Gao, Q. QoS Performances of IEEE 802.11 EDCA and DCF: A Testbed Approach. In Proceedings of the 5th International Conference on Wireless Communications, Networking and Mobile Computing, Beijing, China, 24–26 September 2009; pp. 1–5.

18) Babalola, O.P.; Balyan, V. Vertical Handover Prediction Based on Hidden Markov Model in Heterogeneous VLC-WiFi System. Sensors 2022, 22, 2473.

19) Pohle, J.; Langrock, R.; van Beest, F.M.; Schmidt, N.M. selecting the number of states in hidden markov models: Pragmatic solutions illustrated using animal movement. J. Agric. Biol. Environ. Stat. 2017, 22, 270–293.

20) Berkhin, P. A survey of clustering data mining techniques. Group Multidiscip. Data 2006, 1, 25–71.